Theoretical Chemistry Accounts (2018) 137:91
https://doi.org/10.1007/s00214-018-2276-2

REGULAR ARTICLE

A theoretical study of the reaction mechanism and rate constant of C_4H ($\tilde{X}^2\Sigma^+$) + C_2H_6

Ruiping Huo[1] · Xiang Zhang[2] · Xuri Huang[3] · Tao Zhang[1]

Received: 4 January 2018 / Accepted: 11 June 2018 / Published online: 15 June 2018

Abstract

Theoretical investigations have been carried out on the mechanisms and kinetics of the reaction of linear butadiynyl radical with ethane at the CCSD(T)/aug-cc-pVTZ//ωB97X-D/6-311++G(3*df*,2*p*) level. Four hydrogen abstraction channels (***M1a***, ***M1b***, ***M2a*** and ***M2b***) were investigated. The calculated results indicate that two competitive channels ***M1a*** and ***M1b*** are the predominant mechanisms, while ***M2a*** and ***M2b*** are unfavorable due to the higher barriers. The canonical variational transition state theory (CVT) with the small-curvature tunneling correction (SCT) was utilized to calculate the rate constants for ***M1a*** and ***M1b***. The reactant side wells along the two reaction paths (***M1a*** and ***M2b***) were found and considered in chemical kinetic calculations. The three-parameter rate constant expressions are fitted over a wide temperature range of 145–1000 K.

Keywords Butadiynyl radical · Ethane · Molecular orbital · Rate constants

1 Introduction

The monohydrogenated linear butadiynyl radical C_4H is an important intermediate and plays a significant role in planetary atmospheres and combustion reactions [1–3]. The C_4H radical has been found in abundance in interstellar space than other small molecules [2–4]. It is an essential precursor for the formation of polycyclic aromatic hydrocarbons and fullerenes [1–3, 5]. The C_4H was first synthesized in 1975 in low temperature (4 K) argon and neon noble gas matrices after the UV photolysis of diacetylene [6]. And it was identified again in the carbon-rich star IRC + 10216 [7] as well as in dense clouds in 1978 [8]. Many studies found that there were two low-lying electronic states ($\tilde{X}^2\Sigma^+$ and $\tilde{A}^2\Pi$) for C_4H molecule. The $\tilde{X}^2\Sigma^+$ and $\tilde{A}^2\Pi$ are the ground state and the lowest excited state, respectively [1, 6, 9–11]. The dipole moment of the ground state C_4H ($\tilde{X}^2\Sigma^+$) is about 0.87 Debye, that is much smaller than the $\tilde{A}^2\Pi$ one. In recent years, the gas phase kinetics of reactions of the linear butadiynyl radical C_4H with a series of compounds have gained extensive attention due to its potential importance [1, 5, 12, 13]. Experimental investigations for C_4H radical reactions with various hydrocarbons among the most abundant observed in Titan's atmosphere have been reported [14–16]. The theoretical study of the C_4H radical with a series of compounds, such as CH_4, CH_3OH, H_2, C_2H_4, and C_4H_{10} has been done by three study groups [17–21]. However, to the best of our knowledge, there is no available theoretical study of $C_4H + C_2H_6$. In this paper, we have investigated the reaction of C_4H with C_2H_6 using the density functional theory. Owing to different relative configurations in attacking process, four plausible reaction mechanisms are suggested. Depending on our calculated results, we obtained that ***M1a*** and ***M1b*** are the most effective reaction pathways.

Dr. Xuri Huang and Dr. Tao Zhang are the co-authors for this work.

Electronic supplementary material The online version of this article (https://doi.org/10.1007/s00214-018-2276-2) contains supplementary material, which is available to authorized users.

✉ Ruiping Huo
ruipinghuo@tynu.edu.cn

1 School of Physics, Jilin University, Changchun 130023, People's Republic of China

2 School of Chemistry and Materials Science, Shanxi Normal University, Linfen 041004, People's Republic of China

3 Institute of Theoretical Chemistry, Jilin University, Changchun 130023, People's Republic of China

2 Computational methods

All the electronic structural calculations were performed by Gaussian09 program [22]. The geometries involved in the title reaction were optimized at the ωB97X-D/6-311++G(3*df*,2*p*) level of theory [23]. Frequency calculations were carried out at the same level to characterize the nature of the computed stationary points. All the reactants, pre-reactive complexes and products were identified with zero imaginary frequency. All transition states presented in this work were marked with one and only one imaginary frequency. Intrinsic reaction coordinate (IRC) [24, 25] calculations were carried out using ωB97X-D/6-311++G(3*df*,2*p*) level of theory to verify that the transition states connect the designated local minima. The coupled-cluster (CC) theory [26] of triple excitations CCSD(T) method [27] with the aug-cc-pVTZ basis sets was used to obtain more accurate reaction energies for all species using the ωB97X-D-optimized geometries.

The Polyrate 9.7 program [28] was employed to calculate the thermal rate constants using the conventional transition state theory (TST) [29], canonical variational transition state theory (CVT) [30, 31], and canonical variational transition state including a small-curvature tunneling correction (CVT/SCT) method [29] over the wide temperature range of 145–1000 K. The pre-reactive complexes (**Rc1a** and **Rc1b**) were considered in the chemical kinetic calculations. **TS1a** and **TS1b** have two low vibrational frequencies, one is a torsional mode and the other is a bending vibration. In kinetic calculations, the torsional modes of **TS1a** (74 cm^{-1}) and **TS1b** (72 cm^{-1}) were treated by the hindered-internal-rotator approximation [VANHAR, TOR]; the low-frequencies bending modes of **TS1a** (51 cm^{-1}) and **TS1b** (55 cm^{-1}) were treated by semi-classical WKB with a quadratic–quartic fit to potential [VANHAR, QQSEMI], while all the other modes are treated by the default harmonic approximation." Besides, frontier molecular orbital of selected points along the molecular electrostatic potential (MEP) was performed by ORCA 2.8 program package [32] and plotted using Chimera [33].

3 Results and discussion

3.1 Electronic structure calculations

The $C_4H + C_2H_6$, two H-abstraction mechanisms (***M1*** and ***M2***) are considered. ***M1*** is defined that the hydrogen abstraction by C^1 of C_4H and ***M2*** is the hydrogen abstraction by C^4 of C_4H. Owing to C_4H and C_2H_6 attacking each other in a different direction, each mechanism ***M1*** and ***M2*** has two reaction channels ***M1a*** and ***M1b, M2a*** and ***M2b***, respectively.

M1: hydrogen abstraction by C^1 of C_4H

$$\cdot C^1 \equiv C^2 - C^3 \equiv C^4H + C_2H_6 \rightarrow H^1C \equiv C^2 - C^3 \equiv C^4H + \cdot C_2H_5 \ (M1a,\ M1b)$$

M2: hydrogen abstraction by C^4 of C_4H

$$\cdot C^1 \equiv C^2 - C^3 \equiv C^4H + C_2H_6 \rightarrow C^1 \equiv C^2 - C^3 \equiv C^4H_2 + \cdot C_2H_5 \ (M2a,\ M2b)$$

The optimized geometries of reactants, pre-reactive complexes, transition states and products involved in above reaction mechanisms, with the selected bond lengths and bond angles at the ωB97X-D/6-311++G(3*df*,2*p*) level, are presented in Fig. 1. The coordinates of the reactants, pre-reactive complexes, transition states and products are provided in Supplementary material coord-xyz. The distances of forming and breaking C–H bonds in four transition states (**TS1a**, **TS1b**, **TS2a** and **TS2b**) are given in Table 1. From Table 1, one can see that the breaking C5–H1 bond in **TS1a**, **TS1b**, **TS2a** and **TS2b** is elongated by 4.7, 4.1, 31.5 and 30.3%, as compared to the C5–H1 equilibrium bond length in C_2H_6, respectively, and the forming C1/C4–H1 bonds in **TS1a**, **TS1b**, **TS2a** and **TS2b** are longer than the equilibrium bond length of C1/C4–H1 in HC_4H/C_4H_2 by 55.4, 57.8, 16.7 and 17.3%, respectively. These structural studies reveal that **TS1a** and **TS1b** are more reactant-like, while **TS2a** and **TS2b** are more product-like. Transition states **TS1a**, **TS1b**, **TS2a** and **TS2b** possess one and only one imaginary frequency 255*i*, 208*i*, 1009*i* and 1113*i* cm^{-1}, respectively, indicating that the TSs are real first-order saddle point (see Table S1). Structural characteristics and values of the imaginary frequency indicate that **TS1a** and **TS1b** are loose transition states, while **TS2a** and **TS2b** are tight transition states.

Figure 2 shows the barrier heights of four reaction channels obtained at the CCSD(T)/aug-cc-pVTZ//ωB97X-D/6-311++G(3*df*,2*p*) level. Electronic structure energies ($\mathbf{E_{elec}}$), sum of electronic and zero-point energies ($\mathbf{E_{elec} + ZPE}$), sum of electronic and thermal Enthalpies ($\mathbf{E_{elec} + H_{corr}}$) for various species at the ωB97X-D/6-311++G(3df,2p) level are listed in Table S2. Two isolated reactant molecules ($C_4H + C_2H_6$) are used to define reference energy (0.0 kcal/mol). As shown in Figs. 1 and 2, the C^1 atom of the liner C_4H can attach to one of H atoms of C_2H_6, resulting in **Rc1a** and **Rc1b**. The shapes of **Rc1a** and **Rc1b** are *cis*-like structure and *trans*-like structure, respectively. The relaxed potential energy surface (PES) scans along the distance between the H atom in C_2H_6 and C^1 atom of C_4H show that this process is no barrier. The scan results indicate that the **Rc1a** and **Rc1b** are the initial adducts. Both **Rc1a** and **Rc1b** are also connected to the **P1** ($HC_4H + \cdot C_2H_5$) through the reactant-like transition states **TS1a** and **TS1b**, respectively. Intrinsic reaction path (IRC) calculations revealed

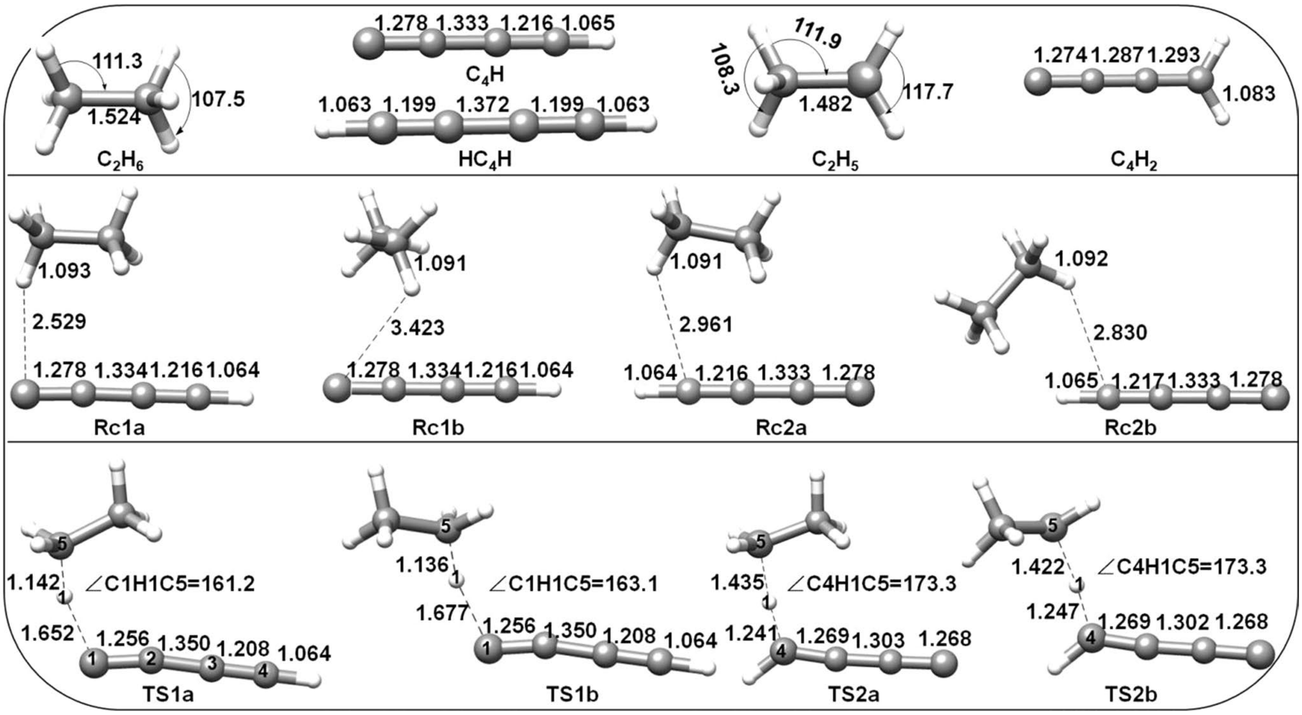

Fig. 1 Geometric parameters of various species involved in the title reaction at the ωB97X-D/6-311++G(3*df*,2*p*) level. Bond length in unit of angstrom and angle in unit of degree

Table 1 The distances of forming C1/C4–H1 bond and breaking C5–H1 bond in various transition states and the elongated ratio of compared with the corresponding values in the reactants and products

Species	C1/C4–H1 (Å)	C5–H1 (Å)
TS1a	0.589 (55.4%)	0.051 (4.7%)
TS1b	0.614 (57.8%)	0.045 (4.1%)
TS2a	0.178 (16.7%)	0.344 (31.5%)
TS2b	0.184 (17.3%)	0.331 (30.3%)

that ***M1a*** and ***M1b*** involve reactant side complexes **Rc1a** and **Rc1b** with relative energy of − 1.2 and − 1.4 kcal/mol, before **TS1a** and **TS1b**, respectively. The C^4 atom of the liner C_4H can attach to one of H atoms of C_2H_6, resulting in **Rc2a** and **Rc2b**. The shapes of **Rc2a** and **Rc2b** are *cis*-like structure and *trans*-like structure, respectively. Both **Rc2a** and **Rc2b** are also connected to the **P3** ($C_4H_2 + \cdot C_2H_5$) through the reactant-like transition state **TS2a** and **TS2b**, respectively. The relative free energies of four transition

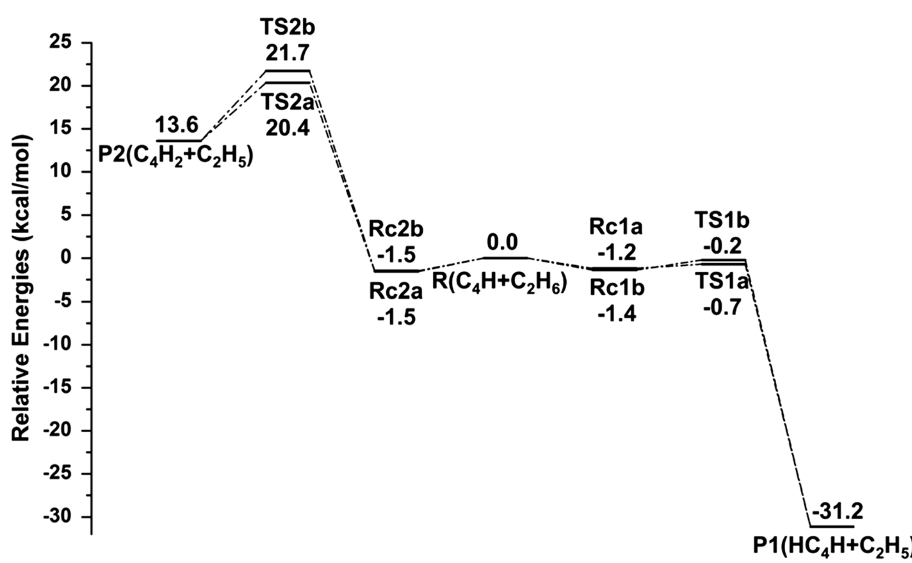

Fig. 2 Relative energy profiles for the title reaction at the CCSD(T)/aug-cc-pVTZ//ωB97X-D/6-311++G(3*df*,2*p*) level, in units of kcal/mol

states **TS1a**, **TS1b**, **TS2a** and **TS2b** were calculated to be −0.7, −0.2, 20.4 and 21.7 kcal/mol, respectively, at the CCSD(T)/aug-cc-pVTZ//ωB97X-D/6-311++G(3*df*,2*p*) level. Moreover, ***M1*** is exothermic by 31.2 kcal/mol, but ***M2*** is endothermic by 13.6 kcal/mol. The C^1 atom in the C_4H radical was demonstrated to be the most reactive site and ***M1a*** and ***M1b*** are mainly two competitive reaction pathways. ***M2*** is kinetically less favorable owing to the much higher energy barriers compared to ***M1*** and, thus, its contribution to the overall reaction is almost negligible and will not be discussed in the kinetic calculations.

3.2 Electron transfer behaviors

Direct electron transfer behaviors of ***M1a*** and ***M1b*** are investigated by quasi-restricted orbital. Figure 3 displays the schematic frontier molecular orbital diagrams for the reactants, transition states, and products involved in ***M1a*** and ***M1b***. Figure 4 presents the changes in the spin density distribution of key atoms in ***M1a***(a) and ***M1b***(b). As shown in Fig. 3, on can see that at the starting point, there is a single unpaired electron in π_{C-C} orbital of the C_4H fragment. As the C_4H and C_2H_6 approach each other gradually, the σ_{C-H} bond of C_2H_6 is going to attack the half-occupied π_{C-C} orbital in C_4H radical. The β electron in the C–H bond of C_2H_6 transitions to the single unpaired π_{C-C} orbital of the C_4H fragment and leading to the $\cdot C_2H_5$ fragment with one α electron left. From Fig. 4, one can see that DFT computations of ***M1a*** or ***M1b***, demonstrate that C_4H is spin carriers; 40, 27 and 26% of spin density resides on the C2, C1 and C4 atom, respectively. Along the MEP of ***M1a*** or ***M1b***, the spin density on the H1 and C3 has almost no change, with the density on C5 decrease and that on C1, C2 and C4 increase. Molecular orbital calculations suggest that ***M1a*** and ***M1b*** are typical hydrogen atom transfer (HAT) mechanism.

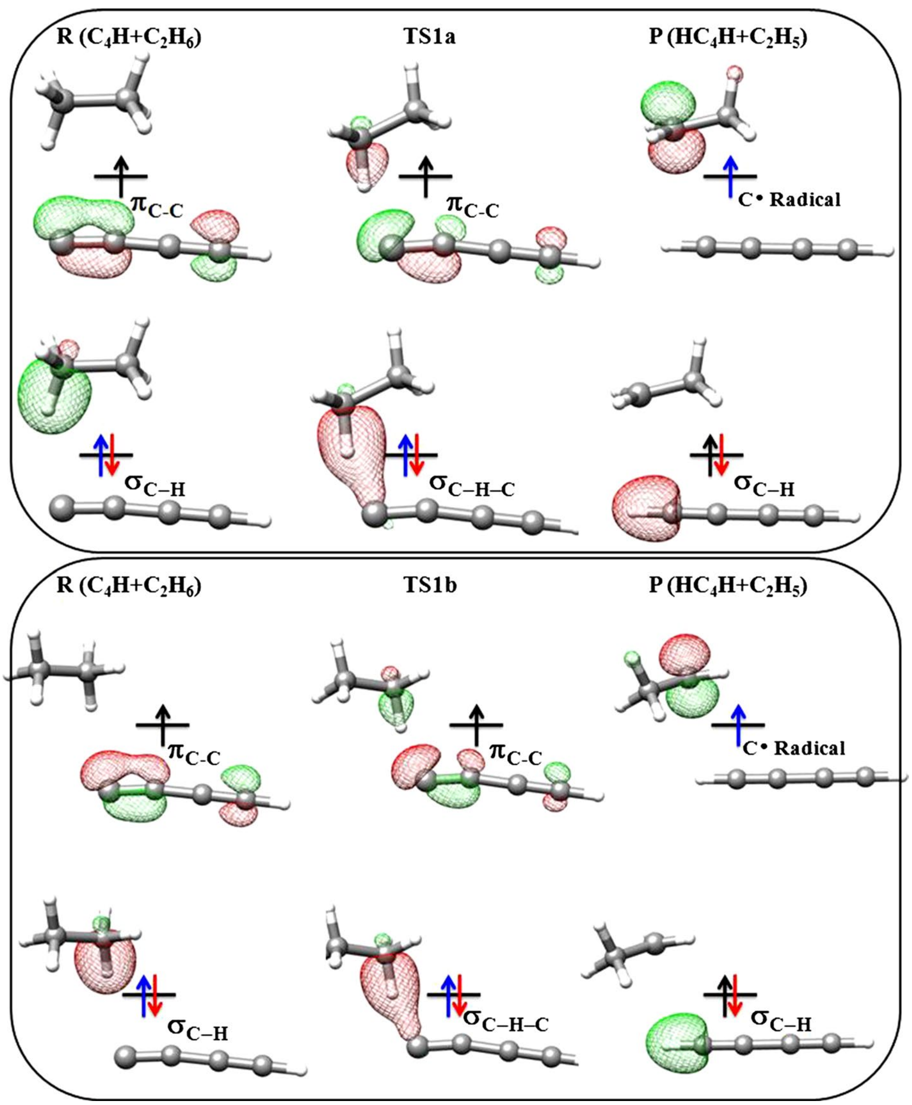

Fig. 3 Schematic MO diagrams of reactants ($C_4H + C_2H_6$), transition states (**TS1a** and **TS1b**) and products ($HC_4H + C_2H_5$)

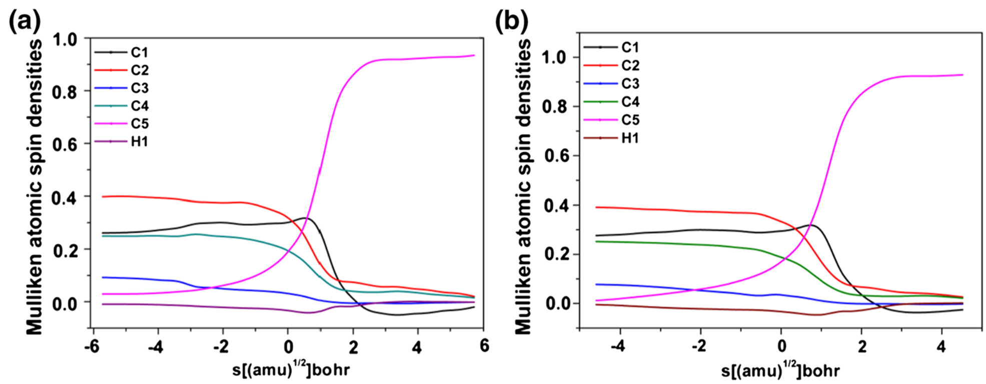

Fig. 4 The change of atomic spin densities on C1, C2, C3, C4 and H1 atom in ***M1a***(a) and ***M2a***(b) obtained from selected points on IRC pathways

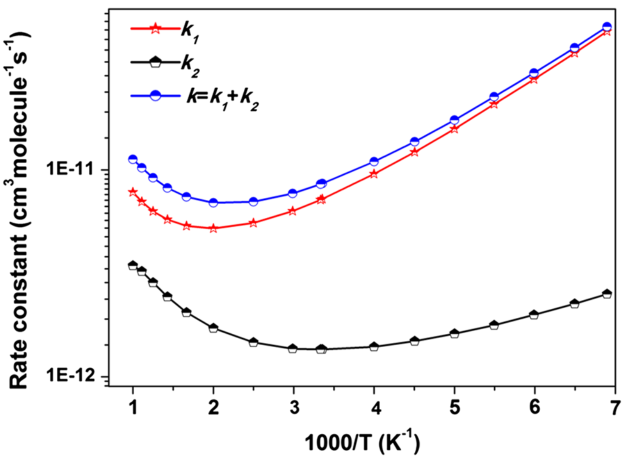

Fig. 5 Plot of the calculated individual CVT/SCT rate constants k_1, k_2 and the overall rate constant ($k=k_1+k_2$), at the CCSD(T)/aug-cc-pVTZ//ωB97X-D/6-311++G(3*df*,2*p*) level versus 1000/*T* between 145 and 1000 K

3.3 Dynamics calculations

The rate constants for the most favorable reaction pathways (***M1a*** and ***M1b***) are calculated using canonical variational transition state theory with small-curvature tunneling corrections (CVT/SCT). The symmetry numbers of C_2H_6, C_4H, TS1a, C_2H_5 and HC_4H are 6, 1, 1, 1 and 2, respectively ($\sigma_{C2H6}=6$, $\sigma_{C4H}=1$, $\sigma_{TS1a}=1$, $\sigma_{C2H5}=1$ and $\sigma_{HC4H}=2$); therefore, the equivalent reaction channels of the forward and reverse reactions are 6 and 2, respectively [SIGMAF=6, SIGMAR=2]. The predicted rate constants in the temperature range 145–1000 K are plotted as functions of the reciprocal of temperature as shown in Figs. S2 and S3 for ***M1a*** and ***M1b***, respectively. And the CVT/SCT rate constants k_1 (***M1a***), k_2 (***M1b***) and the overall rate constant k ($k=k_1+k_2$) are plotted against 1000/*T* (k^{-1}) as shown in Fig. 5. The overall CVT/SCT rate constants are also available by summing up the ***M1a*** (k_1) and ***M2a*** (k_2). These data and the existing experimental rate constants [14, 16] are listed in Table S3. In Fig. S2, the rate constants for TST and CVT are in good agreement with each other in the whole studied temperatures, while CVT and CVT/SCT curves of ***M1a*** have some differences. These results suggest that the variational effect in the whole temperature range is almost negligible, while the small-curvature tunneling correction plays a very important role.

Furthermore, from Fig. S2 one can see that the rate constants significantly increase as the temperature decrease, indicating negative temperature dependence in temperature range 145–500 K. In Fig. S3, the rate constants of TST and CVT are nearly same over the whole temperature range, which means that the variational effect for ***M1b*** is very small and almost negligible. The CVT rate constants are obviously greater than those of the CVT/SCT values in the 800–1000 K. For example, the $k_{CVT}/k_{CVT/SCT}$ for ***M1b*** is 1.11 and 1.30 at 800 and 1000 K, respectively. Therefore, SCT correction plays an important role and should be considered in rate constant calculations in high-temperature range. It is clear that in this reaction there is negative temperature dependence at temperatures smaller than 298 K. From Table S3, we can see that the deviation between the theoretical and experimental values is 1.2, 4.8 and 4.8 times at 145, 298 and 300 K, respectively. The present calculated rate constants are less than the available experimental values. A possible explanation for this discrepancy may result from the basis set size and the frequency mode in the transition state calculation. Therefore, calculation at the CCSD(T) level with larger basis sets (extremely consuming CPU time and memory capacities) may tend to decrease the discrepancy, but it is not guaranteed.

The three-parameter (k^3) rate-temperature expression fitting of the overall CVT/SCT rate constants are performed for convenience of future experimental measurements. (in units of cm^3 $molecule^{-1}$ s^{-1}).

$$k^3(145-200\,\mathrm{K}) = 6.38\times10^{-16}(T)^{1.22}\exp\left(-\frac{754.29}{T}\right)$$

$$k^3(200-300\,\mathrm{K}) = 2.21\times10^{-17}(T)^{1.76}\exp\left(-\frac{854.51}{T}\right)$$

$$k^3(300 - 1000\,\mathrm{K}) = 2.77 \times 10^{-18}(T)^{2.07} \exp\left(-\frac{942.04}{T}\right)$$

4 Conclusion

Reaction mechanisms of linear butadiynyl radical with ethane are investigated at the CCSD(T)/aug-cc-pVTZ//ωB97X-D/6-311++G(3*df*,2*p*). Four hydrogen abstraction channels are considered. Calculated results show that ***M1a*** and ***M1b*** are the main and competitive channels. Orbital analysis shows that ***M1a*** and ***M1b*** are the H atom abstraction mechanism. The conventional transition state theory (TST), canonical variational transition state theory (CVT) and canonical variational transition state including a small-curvature tunneling correction (CVT/SCT) method are used to calculate the rate constants for ***M1***(***M1a*** and ***M1b***) at the CCSD(T)/aug-cc-pVTZ//ωB97X-D/6-311++G(3*df*,2*p*) levels of theory over a wide temperature range of 145–1000 K. The calculated results show that for ***M1a***, the small-curvature tunneling correction is important and the variational effect is negligible. For ***M1b***, the variational effect is insignificant in the whole temperature range, while the SCT is very important and should be taken into account in the rate constant calculations in high-temperature range. Three-parameter Arrhenius expressions are also provided within 145–1000 K.

Acknowledgements The authors are grateful for the reviewers' invaluable comments.

References

1. Kiefer JH, Sidhu SS, Kern RD, Xie K, Chen H, Harding LB (1992) Combust Sci Technol 82:101–130
2. Millar TJ, Farquhar PRA, Willacy K (1997) Astron Astrophys Suppl Ser 121:139–185
3. Steven DD, Chun Ming L (1998) Astrophys J 502:898–908
4. Hoshina K, Kohguchi H, Ohshima Y, Endo Y (1998) J Chem Phys 108:3465–3478
5. Zhang HY, McKinnon JT (1995) Combust Sci Technol 107:261–300
6. Dismuke KI, Graham WRM, Weltner W (1975) J Mol Spectrosc 57:127–137
7. Guelin M, Greenan S, Thaddeus P (1978) ApJ Lett 224:27
8. Friberg P, Hjalmarson A, Irvine WM (1980) ApJ Lett 241:99
9. McCarthy MC, Gottlieb CA, Thaddeus P, Horn M, Botschwina P (1995) J Chem Phys 103:7820–7827
10. Woon DE (1995) Chem Phys Lett 244:45–52
11. Mazzotti FJ, Raghunandan R, Esmail AM, Tulej M, Maier JP (2011) J Chem Phys 134:164303
12. Hausmann M, Homann KH (1991) In: Combust React Kinet, pp 22/1–22/12
13. Kanamori H, Hirota E (1988) J Chem Phys 89:3962–3969
14. Berteloite C, Le Picard SD, Balucani N, Canosa A, Sims IR (2010) Phys Chem Chem Phys 12:3666–3676
15. Berteloite C, Le Picard SD, Balucani N, Canosa A, Sims IR (2010) Phys Chem Chem Phys 12:3677–3689
16. Berteloite C, Le Picard SD, Birza P, Gazeau M-C, Canosa A, Bénilan Y, Sims IR (2008) Icarus 194:746–757
17. Huo RP, Zhang X, Huang XR, Li JL, Sun CC (2011) J Phys Chem A 115:3576–3582
18. Huo RP, Zhang X, Zhang CF (2015) Chem Phys Lett 620:82–87
19. Huo RP, Zhang X, Huang XR, Li JL, Sun CC (2013) Acta Chim Sinica 71:743–748
20. Kim J, Ihee H (2012) Int J Quantum Chem 112:1913–1925
21. Yu AY, Zhang HX (2013) Comput Theor Chem 1019:101–107
22. Frisch MJ, Trucks GW, Schlegel HB, Scuseria GE, Robb MA, Cheeseman J R, Scalmani G, Barone V, Mennucci B, Petersson GA, Nakatsuji H, Caricato M, Li X, Hratchian HP, Izmaylov AF, Bloino J, Zheng G, Sonnenberg JL, Hada M, Ehara M, Toyota K, Fukuda R, Hasegawa J, Ishida M, Nakajima T, Honda Y, Kitao O, Nakai H, Vreven T, Montgomery, JA Jr., Peralta JE, Ogliaro F, Bearpark M, Heyd JJ, Brothers E, Kudin KN, Staroverov VN, Kobayashi R, Normand J, Raghavachari K, Rendell A, Burant JC, Iyengar SS, Tomasi J, Cossi M, Rega N, Millam JM, Klene M, Knox JE, Cross JB, Bakken V, Adamo C, Jaramillo J, Gomperts R, Stratmann RE, Yazyev O, Austin AJ, Cammi R, Pomelli C, Ochterski JW, Martin RL, Morokuma K, Zakrzewski VG, Voth GA, Salvador P, Dannenberg JJ, Dapprich S, Daniels AD, Farkas O, Foresman JB, Ortiz JV, Cioslowski J, Fox DJ (2009) Gaussian, Inc., Wallingford CT Gaussian 09, Revision A.01
23. Chai J-D, Head-Gordon M (2008) Phys Chem Chem Phys 10:6615–6620
24. Gonzalez C, Schlegel HB (1989) J Chem Phys 90:2154–2161
25. Gonzalez C, Schlegel HB (1991) J Chem Phys 95:5853–5860
26. Scuseria GE, Schaefer HF (1989) J Chem Phys 90:3700–3703
27. Pople JA, Gordon MH, Raghavachari K (1989) J Chem Phys 87:5968–5975
28. Corchado JC, Chuang YY, Past PL, Hu WP, Liu YP, Lynch GC, Nguyen KA, Jackels CF, Fernandez-Ramos A, Ellingson BA, Lynch BJ, Zheng JJ, Melissas VS, Villa J, Rossi I, Coitino EL, Pu JZ, Albu TV, Steckler R, Garrett BC, Isaacson AD, Truhlar DG (2007) POLYRATE, version 9.7. University of Minnesota, Minneapolis
29. Liu YP, Lynch GC, Truong TN, Lu DH, Truhlar DG, Garrett BC (1993) J Am Chem Soc 115:2408–2415
30. Garrett BC, Truhlar DG (1979) J Chem Phys 70:1593–1598
31. Garrett BC, Truhlar DG (1979) J Am Chem Soc 101:4534–4548
32. Neese F ORCA -an ab initio, density functional and semiempirical program package Version 2.8, Bonn University
33. Pettersen EF, Goddard TD, Huang CC, Couch GS, Greenblatt DM, Meng EC, Ferrin TE (2004) J Comput Chem 25:1605–1612